Sensitivity of Thermal Infrared Radiation at the Top of the Atmosphere and the Surface to Ice Cloud Microphysics

Philippe Dubuisson, Vincent Giraud, Jacques Pelon, Bertrand Cadet, Ping Yang

Sensitivity of Thermal Infrared Radiation at the Top of the Atmosphere and the Surface to Ice Cloud Microphysics

PHILIPPE DUBUISSON

Écosystèmes Littoraux et Côtiers, Université du Littoral Côte d'Opale, Wimereux, France

VINCENT GIRAUD

LaMP, Université Blaise Pascal, Aubière, France

JACQUES PELON

Service d'Aéronomie, Université Pierre et Marie Curie, Paris, France

BERTRAND CADET

Laboratoire de l'Atmosphère et des Cyclones, Université de la Réunion, Saint-Denis de la Réunion, France

PING YANG

Department of Atmospheric Sciences, Texas A&M University, College Station, Texas

(Manuscript received 12 June 2007, in final form 5 March 2008)

ABSTRACT

This paper reports on the sensitivity of the brightness temperatures associated with radiances at the surface and the top of the atmosphere, simulated for the Imaging Infrared Radiometer (IIR) 8.7-, 10.6-, and 12-μm channels under ice cloudy conditions, to the optical and microphysical properties of ice clouds. The 10.6- and 12-μm channels allow simultaneous retrieval of ice cloud optical thickness and effective particle size (D_{eff}) less than 100 μm. It is illustrated that the particle shape and size distributions of ice crystals have noticeable effects on the brightness temperatures. Using the split window technique based on the 10.6- and 12-μm channels in conjunction with cloud properties assumed a priori, the authors show that the influence of the cloud microphysical properties can lead to differences on the order of $\pm$10% and $\pm$25% in retrieved effective particle sizes for small ($D_{\text{eff}} < 20$ μm) and large particles ($D_{\text{eff}} > 40$ μm), respectively. The impact of cloud model on retrieved optical thickness is on the order of $\pm$10%. Different particle habits may lead to $\pm$25% differences in ice water path (IWP). Theoretically, the use of an additional channel (i.e., 8.7 μm) can give a stronger constraint on cloud model and improve the retrieval of D_{eff} and IWP. The present simulations have confirmed that cloud microphysics has a significant impact on the 8.7-μm brightness temperatures mainly because of particle shape. This impact is larger than the errors of the IIR measurements for cloud optical thicknesses (at 12 μm) ranging from 0.3 to 8. Furthermore, it is shown that the characterization of optical and microphysical properties of ice clouds from ground-based measurements is quite challenging. Especially, water vapor in the atmosphere has an important impact on ground-based cloud retrievals. Observation stations at higher altitudes or airborne measurements would minimize the atmospheric effect.

1. Introduction

Ice clouds play an important role in the earth's radiation budget and climate (Liou 1986). Accurate information of their optical properties is critical to assessing the climate effects and feedback associated with these clouds (Stephens et al. 1990). Reflected solar radiation and emitted longwave radiation under cirrus cloudy conditions depend strongly upon the complex microphysical properties of these clouds (Mitchell et al. 1996; Fu et al. 1998, 1999; Chepfer et al. 2001; Baran 2003). Several methods have been developed to infer

Corresponding author address: Philippe Dubuisson, LOA, Université des Sciences et Technologies de Lille, 59655 Villeneuve d'Ascq, France.
E-mail: philippe.dubuisson@univ-lille1.fr

DOI: 10.1175/2008JAMC1805.1

the single-scattering properties of semitransparent clouds from space measurements in the infrared atmospheric window (8–13 μm) (Inoue 1985; Baran et al. 1998; Stubenrauch et al. 1999; Baum et al. 2000). In particular, the split window technique in the infrared atmospheric window allows the estimation of the effective particle size using channels centered approximately at 10.8 and 12 μm (Inoue 1987; Parol et al. 1991; Giraud et al. 1997, 2001; Rädel et al. 2003). The extinction efficiencies of ice crystals (Yang et al. 2001, 2005; Baum et al. 2007) vary with the wavelength in the infrared window with an extinction minimum near 10.5 μm, which is pronounced for small particles. This feature is useful for determining the effective particle size from the split window technique. However, uncertainties associated with the atmospheric parameters and cloud microphysics assumed a priori in the forward radiative transfer simulation involved in inferring cloud properties can affect the retrieved results. For example, Cooper et al. (2003) reported a noticeable impact of cloud boundary variation on the retrieval of effective particle size and optical thickness.

The Cloud-Aerosol Lidar and Infrared Pathfinder Satellite Observations (CALIPSO) mission provides a unique opportunity for retrieving geophysical parameters that are fundamental to accurately quantifying cloud radiative impact (Winker et al. 2003). The Imaging Infrared Radiometer (IIR) measures the radiation emitted in three channels within the infrared atmospheric window (8.7, 10.6, and 12 μm). Moreover, the Cloud-Aerosol Lidar with Orthogonal Polarization (CALIOP) provides the information about cloud vertical profiles. Algorithms based on the split window technique (Chomette et al. 2003; Chiriaco et al. 2004, 2007) have been developed to interpret IIR data. Specifically, the two IIR channels centered at 10.6 and 12 μm allow the retrieval of the effective particle size. Furthermore, the 8.7-μm channel is sensitive to scattering and can be used to improve the characterization of semitransparent clouds from space (Ackerman et al. 1990).

This paper reports on the sensitivity of the simulated brightness temperatures in the IIR channels to the microphysical properties of ice clouds. This effort is aimed at assessing the accuracy of the effective particle size and optical thickness retrieved from the split window technique using two channels centered at 10.6 and 12 μm, and estimating the impact of the microphysical properties of ice clouds (e.g., the shape and size distributions of ice crystals) on the 8.7-μm brightness temperature.

The rest of this paper is organized as follows: in section 2, the cloud properties and models used in simulations are described. The single-scattering properties reported by Yang et al. (2005) for nonspherical ice particles have been used in the present radiative transfer calculations. In section 3 the sensitivity of brightness temperature to cloud model is presented in the context of the split window technique. Brightness temperatures are calculated by accounting for multiple scattering and gaseous absorption on the basis of a fast yet accurate radiative transfer code referred to as FASDOM (Dubuisson et al. 2005). In section 4, the feasibility of retrieving cloud optical and microphysical properties from the three IIR channels is analyzed. Sensitivity studies regarding derived cloud properties are carried out from both spaceborne and ground-based remote sensing perspectives. Finally, the conclusions of this study are given in section 5.

2. Microphysics of ice clouds

a. Optical properties for individual ice particles

In this study seven nonspherical ice crystal habits, namely aggregate, bullet rosette, droxtal, hollow column, plate, solid column, and spheroid are considered on the basis of a scattering database reported by Yang et al. (2005). This database includes the geometrical parameters (projected area A and geometric volume V of the particle) and optical properties (extinction coefficient, single-scattering albedo, phase function, and asymmetry factor) of ice crystals with maximum dimensions ranging from 10 to 10 000 μm in a spectral range of 100–3000 cm^{-1} (3.3–100 μm). The effective particle size D_{eff} (Foot 1988; Mitchell and Arnott 1994; Mitchell 2002; King et al. 2004; Baum et al. 2005a,b) is used in radiative transfer calculations. The effective diameters considered in this study are between 5 and 100 μm, which are in agreement with a recent analysis based on in situ measurements for midlatitude cirrus cloud (Gayet et al. 2006).

Figure 1 shows the variation of the imaginary part of ice refractive index in the 8–13-μm window with data from Warren (1984). The absorbing feature of ice in this spectrum is fundamental to the split window technique based on brightness temperature differences at two thermal infrared channels (Inoue 1985; Parol et al. 1991; Giraud et al. 1997; Rädel et al. 2003). Figure 1 also shows the response functions for the three channels of the Infrared Imaging Radiometer aboard CALIPSO (Winker et al. 2003). For brevity, in the following discussions these channels centered at 8.7, 10.6, and 12 μm are referred to as channels 1, 2, and 3, respectively.

b. Size distribution

There exists no general particle size distribution that can be applied to all ice clouds (Donovan 2003; Ivanova

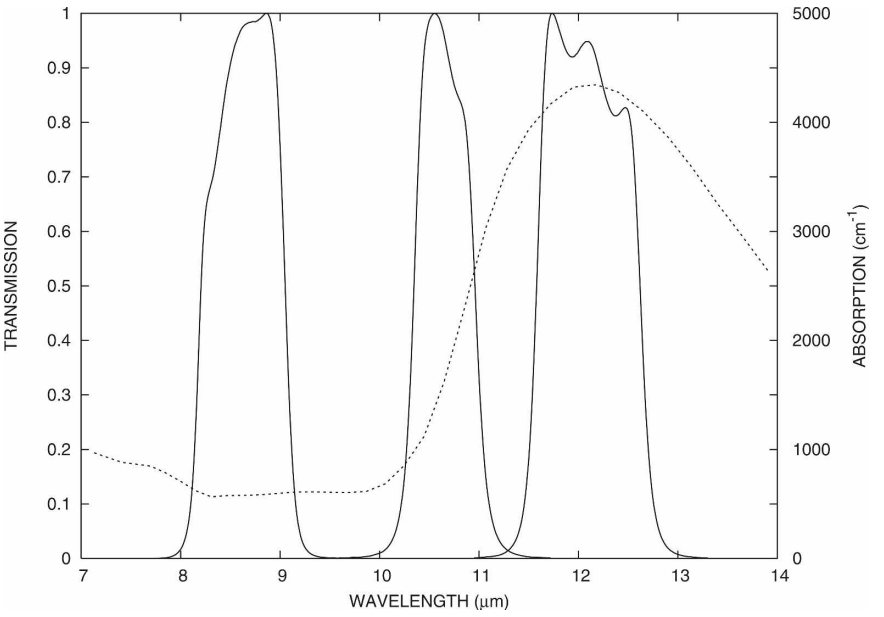

FIG. 1. Spectral response of the three IIR channels onboard CALIPSO. Channels at 8.7, 10.6, and 12 μm are referred to as 1, 2, and 3, respectively, in the text. Spectral variation of the ice absorption (Warren 1984) is also reported (dashed line, right axis).

et al. 2001). Based on observations, ice particle size spectra in cirrus are either monomodal or bimodal (Varley 1978; Arnott et al. 1994; McFarquhar and Heymsfield 1996). In the literature the gamma distribution has been extensively used (e.g., Kosarev and Mazin 1991; Mitchell 1991; Heymsfield et al. 2002; Baum et al. 2005a,b). Here we assume that the size distribution of ice crystals in an ice cloud can be represented by a generalized gamma distribution described by Walko et al. (1995) as follows:

$$n(L) = N\frac{\alpha}{\gamma(\nu)}\lambda^{\alpha\nu-1}L^{\alpha\nu-1}\exp[-(\lambda L)^{\alpha}], \qquad (1)$$

where N is the total concentration of particles per unit volume of air for a nontruncated distribution, λ is the slope parameter, and both α and ν are shape parameters. The parameters ν and α control the relative amount of small particles versus large particles in the distribution and are related to the relative variance of the distribution. The slope parameter λ is a scaling dimension, related to the mean size value via

$$\overline{D} = \frac{\int_0^{\infty} n(L)L\,dL}{\int_0^{\infty} n(L)\,dL} = \frac{\gamma(\nu + 1/\alpha)}{\lambda}. \qquad (2)$$

In this study, four size distributions have then been used, which include

- a monodisperse distribution (i.e., all particles have the same size),
- a monomodal gamma generalized size distribution $n_s(L)$ with $\alpha = 3$ and $\nu = 3$ describing small particles, typical for ice particles in young cirrus clouds with a symmetric distribution,
- a monomodal gamma generalized size distribution $n_l(L)$ with $\alpha = 1$ and $\nu = 4$ for large particles produced by aggregation, and
- a bimodal distribution specified as $n(L) = fn_s(L) + (1 - f)n_l(L)$, where f indicates the fraction of small particles. In this study three values of f have been taken, namely, $f = 0.2$, 0.5, and 0.8.

Furthermore, for individual and monomodal distributions, the seven shapes of particles have been used. For the bimodal distribution, we consider droxtals and plates for small and large particles, respectively.

Following Foot (1988), Mitchell (2002), King et al. (2004), and Baum et al. (2005a,b), the effective particle size D_{eff} for a cloud model with a mixture of two different habits for small and large particles can be defined as follows:

$$\overline{D}_{\text{eff}} = \frac{3}{2}\frac{\int_{L^0}^{L^{\infty}} [fV_s(L)n_s(L) + (1 - f)V_l(L)n_l(L)]\,dL}{\int_{L^0}^{L^{\infty}} [fA_s(L)n_s(L) + (1 - f)A_l(L)n_l(L)]\,dL}, \qquad (3)$$

where $V(L)$ and $A(L)$ are the geometric volume and projected area of a particle with a maximum dimension of L, and f is the percentage of small particles. Note that the subscripts s and l indicate small and large particles, respectively. Evidently, Eq. (3) reduces to a formula suitable for a monomodal size distribution when $f = 1$ or $f = 0$.

The optical properties of individual ice crystals (Yang et al. 2005) are integrated over the size distributions. Furthermore, the bulk optical properties are weighted by the spectral response of the instrument (Fig. 1), following Chou et al. (1999) and Baum et al. (2005b). For example, the cloud optical depth δ can be obtained from the bulk extinction coefficient averaged with a response function as follows:

$$\delta = \pi \frac{\int_{\Delta\nu} \int_{L^0}^{L^\infty} [fQ_{\text{ext},s,\nu}(L)A_s(L)n_s(L) + (1-f)Q_{\text{ext},l,\nu}(L)A_l(L)n_l(L)]r_\nu B_\nu(\theta_0)\, dL\, d\nu}{\int_{L^0}^{L^\infty} [fA_s(L)n_s(L) + (1-f)A_l(L)n_l(L)]\, dL \int_{\Delta\nu} r_\nu B_\nu(\theta_0)\, d\nu}. \quad (4)$$

Ice water path (IWP), defined as the integration of ice water content (IWC) along the vertical thickness of a cloud, is a critical parameter in climate studies. There exists a simple relationship between δ and IWP as a function of the particle effective size (Ebert and Curry 1992; Heymsfield et al. 2003), given by

$$\text{IWP} = \frac{\delta}{a\left(1 + \frac{b}{D_{\text{eff}}}\right)}, \quad (5)$$

where the coefficients a and b can be derived from observations or theoretical simulations. Ebert and Curry (1992) showed that these coefficients depend on the spectral bands for both shortwave or longwave radiation. They assumed that ice crystals could be represented in terms of randomly oriented hexagonal columns for the solar radiation and equivalent ice spheres for infrared radiation. Fu (1996) showed that the use of the effective particle size eliminates the dependence of the extinction or absorption properties on particle shape to a certain extent. However, differences may occur due to different assumptions and treatments in the calculation of ice crystal optical properties (Mitchell 2002). Table 1 lists the coefficients a and b calculated for the IIR channel at 12 μm. Table 1 shows noticeable sensitivity of a and b to particle shape. Evidently, the differences between the extinction and absorption efficiencies for the habits used in this study are smaller if the effective particle size D_{eff} is used, particularly in the cases with small values of D_{eff}. However, there still are significant differences in the optical properties of individual ice crystals in the resonance region (Yang et al. 2005). These differences could largely explain the variations of a and b in Table 1 versus particle habit. It is evident from Eq. (5) that uncertainties of cloud model (i.e., variations of the coefficients a and b) can lead to significant uncertainties in IWP.

TABLE 1. Coefficients a and b linking optical depth to IWP and effective diameter according to Eq. (5), assuming cloud models defined in section 2 and for the IIR channel 3 at 12 μm.

Particle shape	a (m^2 kg^{-1})	b (m)
Aggregate	13.30	211.7
Bullet rosettes	15.44	194.6
Droxtal	4.36	798.0
Hollow column	6.86	427.4
Plate	9.46	323.0
Solid column	8.08	394.7
Spheroid	7.43	473.8

3. Radiative transfer modeling for Infrared Imaging Radiometry

a. Radiative transfer code

In this study we use FASDOM, a fast radiative transfer code developed for simulating the IIR radiances (Dubuisson et al. 2005). This code takes into account both absorption and scattering processes. Gaseous absorption is considered on the basis of the correlated k-distribution method, following Kratz (1995). The Discrete Ordinates Radiative Transfer (DISORT) code developed by Stamnes et al. (1988) is used to account for multiple scattering. The accuracy of FASDOM has been assessed in comparison with a reference code (Dubuisson et al. 1996) for which the radiative transfer equation is solved with DISORT in conjunction with a line-by-line model. Simulations have shown that the accuracy of FASDOM is generally better than 0.1 K in terms of brightness temperature difference. This accuracy is comparable to that of the IIR measurements.

b. Brightness temperature simulation

We simulate nadir-viewed radiances at the three IIR channels and the corresponding brightness tempera-

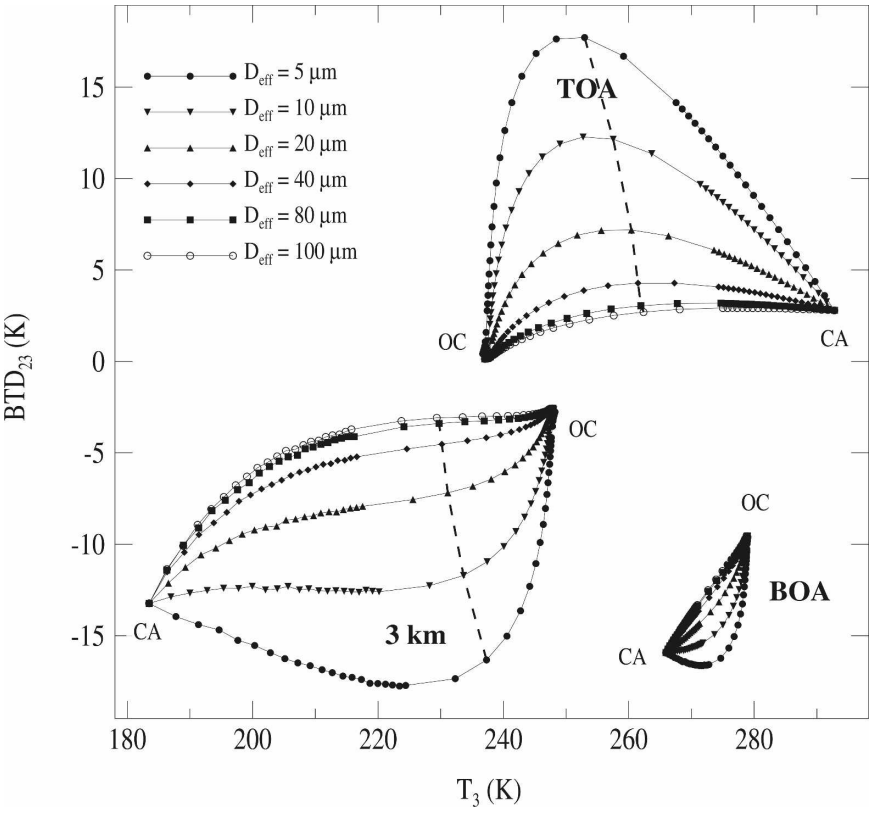

FIG. 2. BTD_{23} as a function of T_3 for a cirrus cloud with various effective sizes D_{eff}, assuming individual ice particles with an aggregate shape. The three sets of arches correspond to simulations performed at the TOA, BOA, and at 3-km altitude (3 km). The cloud is located between 9 and 10 km (237–243 K) for the standard tropical atmosphere from McClatchey et al. (1972). In the arches, CA and OC symbols refer to clear atmosphere and opaque cloud situations, respectively. The vertical dashed lines correspond to an optical depth equal to 2.

tures, assuming that a homogeneous cirrus cloud exists between 9 and 10 km (237–243 K) over the tropics. Temperature and moisture profiles are defined from McClatchey et al. (1972). The surface is assumed to be a blackbody (i.e., the surface emissivity $\varepsilon_s = 1$) with a surface temperature of 299.7 K. The cloud height will be kept constant in this study. Furthermore, the information about cloud-top and cloud-bottom heights and cloud vertical structure is provided a priori. The impact of the uncertainty of cloud-top temperature is discussed in section 4c. In this study, the cloud optical thickness ranges from 0 to 50. The single-scattering properties of ice clouds (δ_{ext}, ϖ_o, g) are derived for the seven ice crystal shapes of Yang et al. (2005) for the four types of size distributions defined in section 2b. Several effective particle sizes ranging from 5 to 100 μm, typical for cirrus clouds, are considered. Note that for D_{eff} larger than 100 μm, the single-scattering properties converge to their asymptotic values.

As an example, the brightness temperature difference between channels 2 and 3 (BTD_{23}) is plotted in Fig. 2 as a function of the brightness temperature of channel 3 (T_3). The nadir-viewed radiances at the top of the atmosphere (TOA), the downwelling radiances at the bottom of the atmosphere (BOA), and at an altitude of 3 km are simulated for the three IIR spectral bands. In the TOA case, Fig. 2 shows arched curves that have been extensively reported in the literature (e.g., Inoue 1985). The maximum BTD value is observed for an optical depth close to 2. These arched curves converge for the two following situations: 1) a clear atmosphere ("CA" in Fig. 2) corresponding to a cloud with an optical thickness of zero, and 2) an opaque cloud ("OC") with an optical thickness larger than 20. The arches are distinguishable and can be used for retrieving cloud effective particle size. Figure 2 also shows similar arches in the BOA and 3-km-height cases. However, the impact of the atmosphere is more important for the BOA observations. In fact, Fig. 2 shows that the lower layers play a crucial role. For the observations made at 3 km, the impact of the lower portion of the atmosphere is relatively small, particularly in the case

of a moist atmosphere. Although cloud characterization seems possible from ground-based measurements, the sensitivity of cloud retrieval to cloud microphysics is substantially diminished for ground-based retrievals in comparison with spaceborne or airborne retrievals. It is also worth noticing that Fig. 2 shows a stronger sensitivity for small cloud optical thicknesses, especially for the observations at 3-km altitude.

c. *Space observations*

Brightness temperature measured at the top of the atmosphere depends strongly on the cloud optical depth at 12 μm ($\delta_{12\mu m}$) and Ice Water Path. As an example, its variation is plotted in Fig. 3 for all the cloud parameters, as functions of $\delta_{12\mu m}$ or IWP. For a fixed optical depth, Fig. 3a shows that the brightness temperature calculated for channel 3 (T_3) is sensitive to the microphysical model. For an optical depth near unity, the brightness temperature variation is approximately 10 K, which is due to the change in microphysical model. The brightness temperatures associated with channels 1 and 2 have similar sensitivities. Figure 3b illustrates the variation of T_3 with IWP, if cloud microphysics is not constrained. From Fig. 3b one can appreciate the importance of constraining the effective particle size that gives the maximum uncertainty, although particle shape also has a significant effect.

Figures 4 and 5 confirm that the BTDs between channels 2 and 3 (BTD_{23}) and 1 and 3 (BTD_{13}) are mainly sensitive to particle size for a given optical depth. Each curve corresponds to a microphysical model, and only the optical thickness varies. The effect of particle size is significant for optical depths between 0.5 and 8. Both Figs. 4 and 5 confirm that the BTDs are mainly sensitive to particle size for optical thicknesses ranging from 0.5 to 8. BTD curves are clearly separated for D_{eff} less than 40 μm and the retrieval of cloud effective size will be accurate for smaller particles. For larger particles, the variations of BTD due to differences in ice cloud model lead to larger uncertainties in the retrievals. The shape of the particles as well as the distribution also has an impact on BT and BTDs. A comparison between Figs. 4a,b shows that the particle shape has a larger effect on the BTD_{23} than the size distribution. Neglecting the size distribution only leads to a small error in the effective particle size. The influence of size distribution is presented in Fig. 4b for aggregates. Individual and monomodal distributions are used in Fig. 4b. The effect of the size distribution on the BTD is on the order of a few tenths of a Kelvin. Furthermore, the impact of a bimodal distribution, defined in section 2, is of the same order. This means that the magnitude of the variation in the BTD is on the order of 1 K (not shown) and may be considered as additional noise in IIR data analysis. Neglecting the size distribution will thus only lead to a small error in the effective particle size. More adequately, the analysis can be done by assuming individual particles whose diameter is equivalent to the one obtained with the distribution. In this case we have to consider a relationship between the equivalent individual particle size and the effective diameter. Size distribution will thus no longer be considered an issue (its impact will however be considered in the calculations).

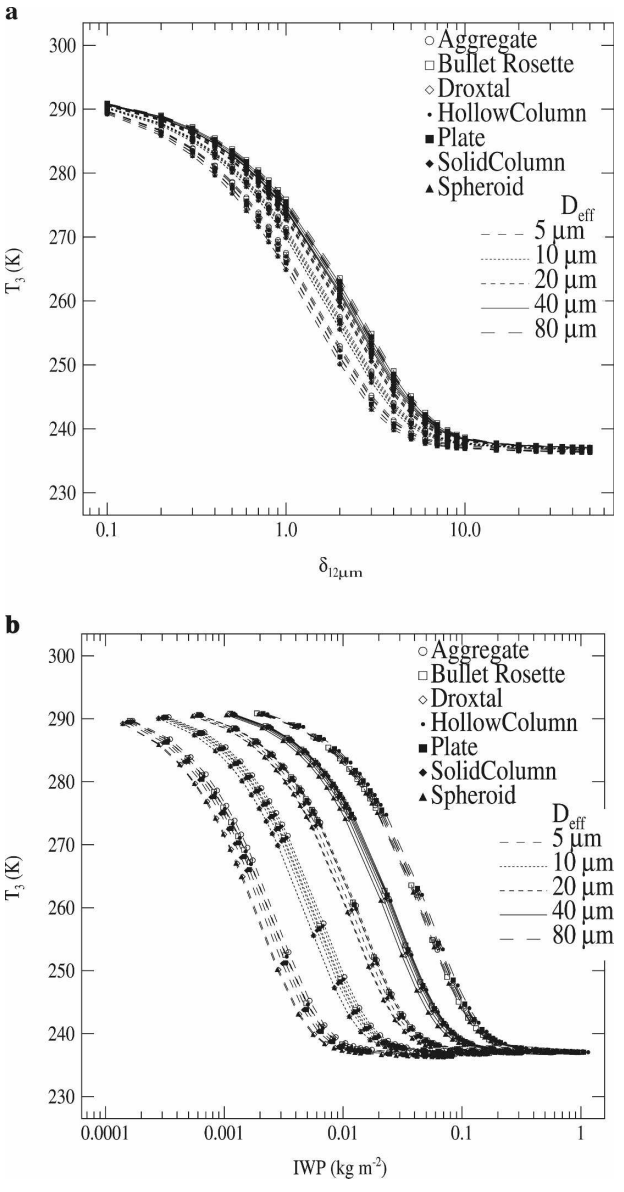

FIG. 3. Dependence of the brightness temperature T_3 at 12 μm on (a) the optical depth $\delta_{12\mu m}$ at 12 μm and (b) IWP for all cloud microphysical models. All particle shapes and effective sizes are considered in calculations, assuming individual ice particles under the same conditions as in Fig. 2.

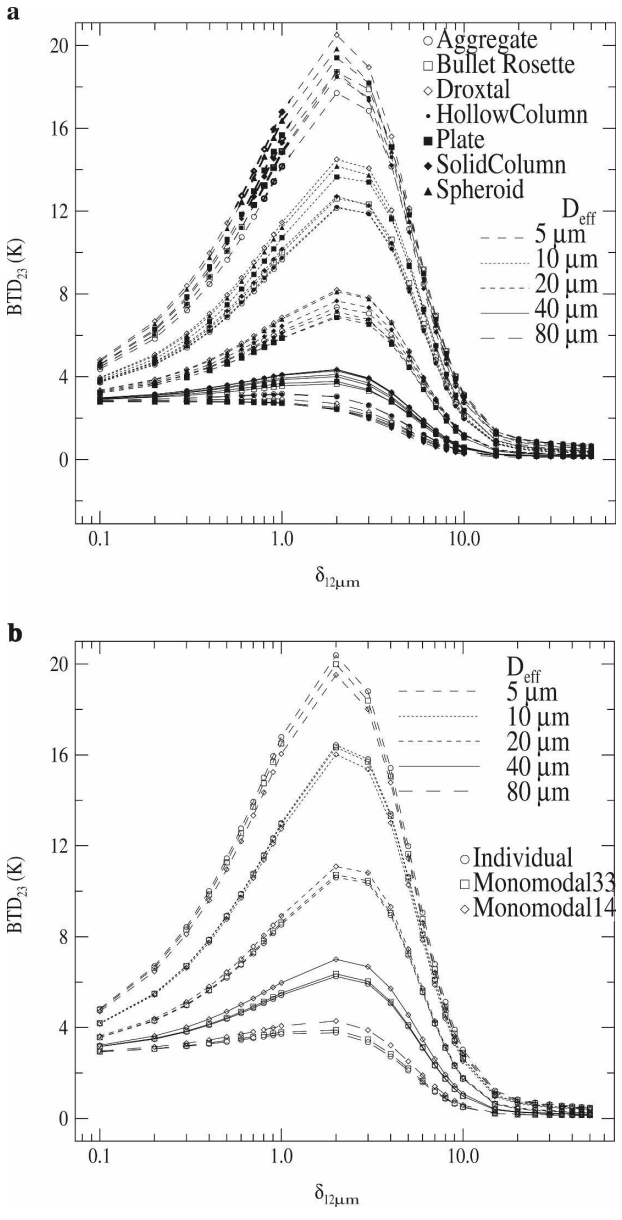

FIG. 4. BTD_{23} at TOA, using channels at 10.6 and 12 μm, as a function of the cloud optical thickness $\delta_{12\mu m}$ at 12 μm. Each curve is representative of a fixed effective size D_{eff} under similar conditions as in Fig. 3. BTDs are presented for the seven particle shapes defined by Yang et al. (2005) assuming (a) individual distribution or (b) 4 different size distributions assuming aggregate shape.

Based on the spectral variations of the single-scattering properties of ice particles (Yang et al. 2005), one can deduce that the absorption effect dominates cloud effect at channels 2 and 3, while the effect of scattering is more important at channel 1. The combination of the three channels should lead to a more accurate retrieval of the effective size and a possible categorization on shapes of the particles.

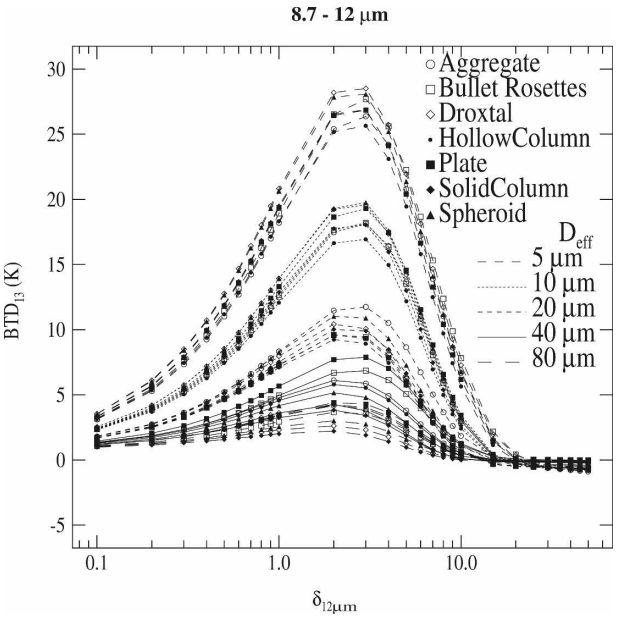

FIG. 5. Same as Fig. 4a, but the BTDs are calculated with channels 1 and 3. Only the dependences with the particle shapes are shown.

d. Ground-based observations

Figure 6 shows BTD curves at the surface. The brightness temperatures associated with downwelling radiances at the IIR channels are calculated with the same atmospheric conditions as those in the preceding discussions. Results for the channels 2 and 3 are shown in Fig. 6 for a set of individual particle shapes (Fig. 6a) and for several size distributions of aggregates (Fig. 6b). Conclusions are rather similar to those derived for nadir observations from space and cloud characterization is possible from BTD at BOA. BTDs are sensitive to the effective particle size, particle shape, and (to a lesser extent) the size distribution. However, the impact of the atmosphere is quite important for ground-based observations.

4. Application to cloud microphysics retrieval

a. Sensitivity of a two-channel effective size and optical thickness retrievals

The set of brightness temperatures simulated at the top of the atmosphere described in section 3b has been used to evaluate the accuracy of the effective size, optical thickness, and IWP retrievals from the two channels centered at 10.6 and 12 μm. Figure 2 shows that the use of the pair of brightness temperatures (T_2, T_3) allows the determination of the optical thickness and effective size of a cloud. However, Fig. 4 also shows that

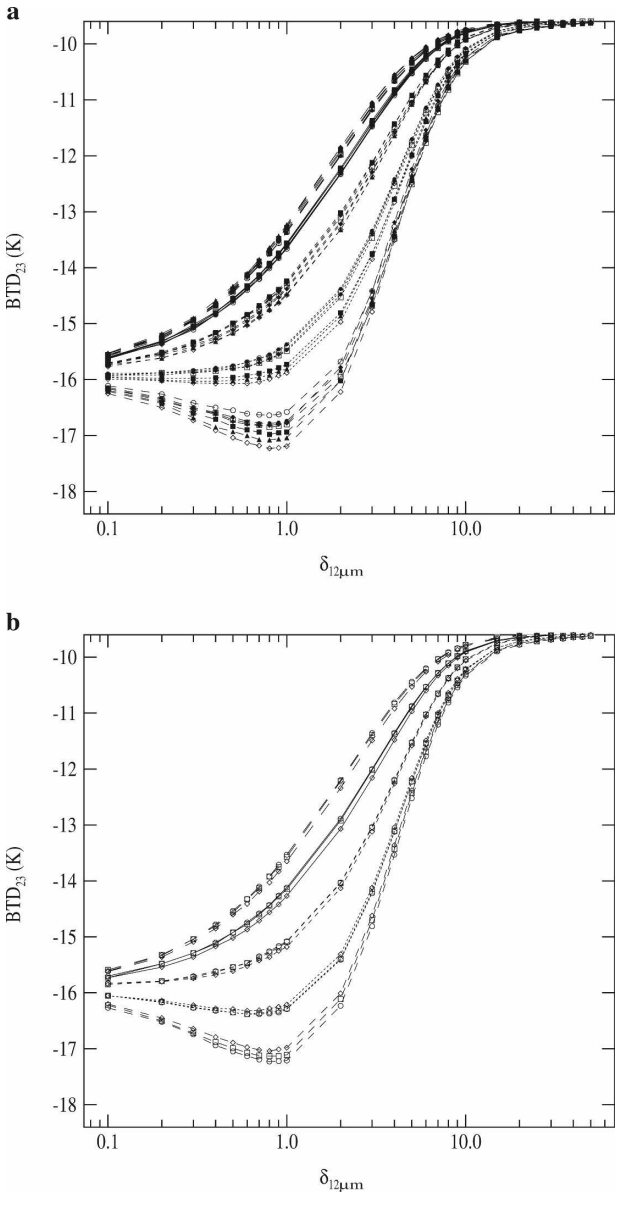

FIG. 6. Same as Fig. 4, but the BTDs are calculated in the case of ground-based observations (BOA).

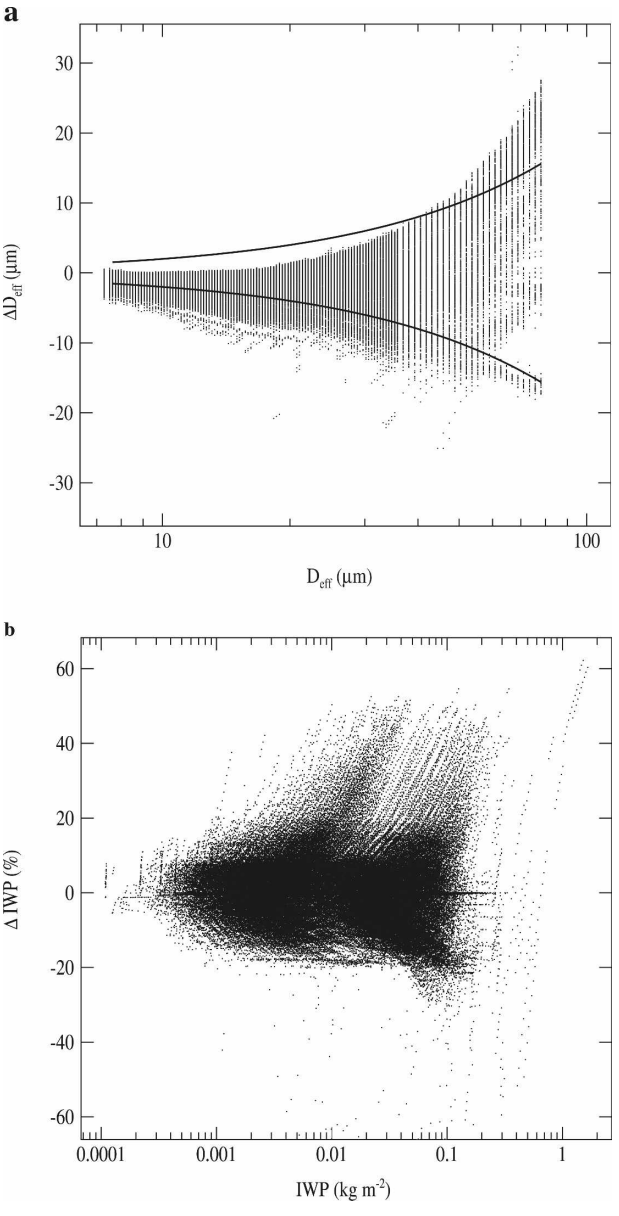

FIG. 7. Influence of the microphysical cloud model (particle shape and size distribution) on (a) the retrieved effective size D_{eff} (Fig. 7a) and (b) the IWP using a split window technique with channels 2 and 3. Solid lines in (a) refer to a relative error of $\pm 20\%$ in D_{eff}. The variation ΔD_{eff} (μm) on the effective size and the relative error ΔIWP (%) are reported for the seven particle shapes defined by Yang et al. (2005), size distributions defined in section 2b, and cloud optical thicknesses ranging from 0 to 50 assuming observations at TOA.

the split window technique based on a fixed pair of brightness temperatures (T_2, T_3) does not correspond to a unique solution because of the influence of the shape of the particles. An iterative procedure has been used to determine the effective size D^i_{eff} and cloud optical thickness $\delta^i_{12\mu\text{m}}$ for each cloud model corresponding to a fixed pair of brightness temperatures (T_2, T_3). In other words, each pair of D^i_{eff} and $\delta^i_{12\mu\text{m}}$ represents a solution to the brightness temperatures T_2 and T_3. To select realistic conditions as an input, the (T_2, T_3) pairs have been selected from simulations, assuming aggregate particle shape for individual ice crystals as the reference calculations. Additional tests (not presented) have shown that changing the particle shape leads to similar conclusions.

This approach has been applied to all optical thicknesses and effective sizes. The results of this effort are shown in Fig. 7. Without an indication on the cloud

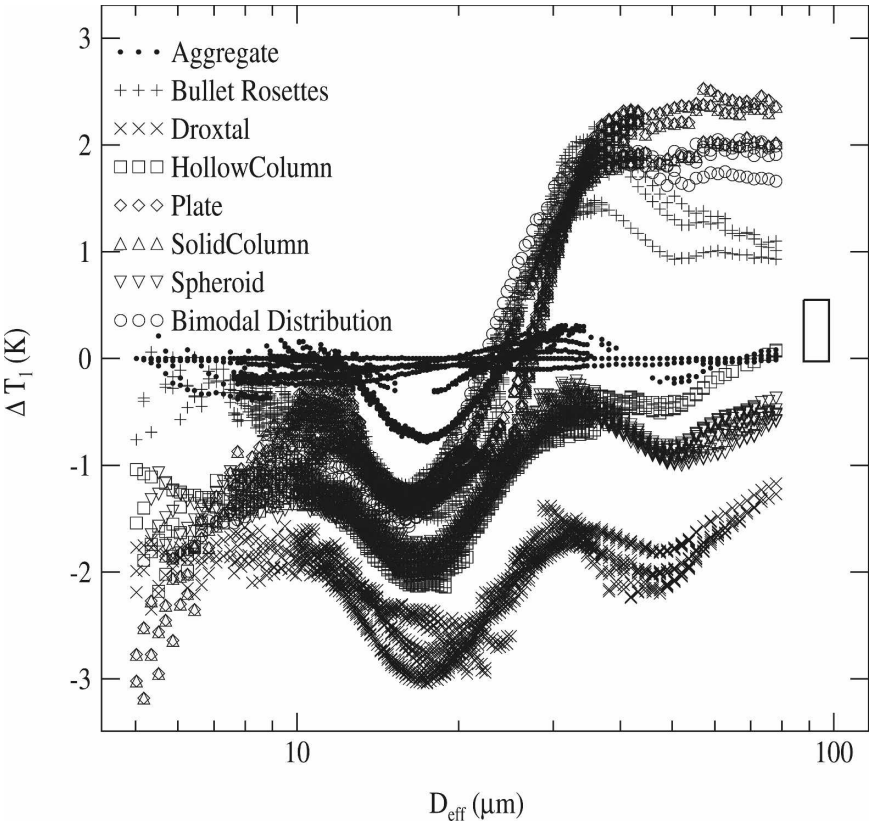

FIG. 8. Deviations ΔT_1 on the brightness temperature at TOA in channel 1 (8.7 μm) due to the cloud microphysical model (particle and size distribution) as a function of the effective size D_{eff}. The aggregate particle shape with individual particle crystal size distribution has been chosen as input for simulations, and deviations ΔT_1 are equal to zero in this case. Optical thickness is equal to 2. The black box represents the error associated with the IIR measurements ($\pm$0.3 K).

particle shape, Fig. 7a shows the uncertainty ΔD_{eff} on the retrieval of the effective particle size D_{eff} as a function of the reference D_{eff} for aggregates. The uncertainty of D_{eff} is on the order of $\pm$15% to $\pm$25% for small ($<$20 μm) and large (up to 80 μm) effective sizes, respectively. In the same manner, the relative uncertainty $\Delta\delta^i_{12\mu\text{m}}$ on the optical thickness at 12 μm has been evaluated. Simulations have shown that $\Delta\delta^i_{12\mu\text{m}}$ is on the order of $\pm$10% for the complete range of optical thickness (not shown). As discussed in section 2b, uncertainties about the optical depth and effective size can lead to errors on the IWP obtained from retrieval algorithms. Figure 7b presents the relative uncertainty ΔIWP due to the particle shape, assuming all shapes and optical thicknesses. Figure 7b shows that ΔIWP increases with IWP. The ΔIWP is on the order of $\pm$5 at low IWP (less than 10^{-4} kg m^{-2}) and increases to $\pm$25% for IWP larger than 10^{-2} kg m^{-2}.

Analyses of these results have shown that these uncertainties are mainly due to the particle shape. The use of a third channel should reduce this uncertainty. Especially, the single-scattering properties at 8.7 μm are very different from those at 10.6 and 12 μm.

b. Contribution of the 8.7-μm channel

It has been shown in the previous section that a pair of brightness temperatures (T_2, T_3) can be simulated from a set of various cloud models defined in terms of D^i_{eff} and $\delta^i_{12\mu\text{m}}$. From Yang et al. (2005) models, all particle optical properties are known for all cloud models at each wavelength. It is then possible to calculate the brightness temperature T^i_1 in the 8.7-μm channel from the cloud optical thickness $\delta^i_{8.7\mu\text{m}}$. The brightness temperature can then be compared to the one assumed as an input for the simulation of T_1. To evaluate the contribution of the channel at 8.7 μm, differences $\Delta T_1 = T_1 - T^i_1$ are reported in Fig. 8 as a function of the effective size for a cloud optical thickness (at 12 μm) of 2 and the aggregate model. As expected, ΔT_1 is equal to zero in the case of the aggregate shape for

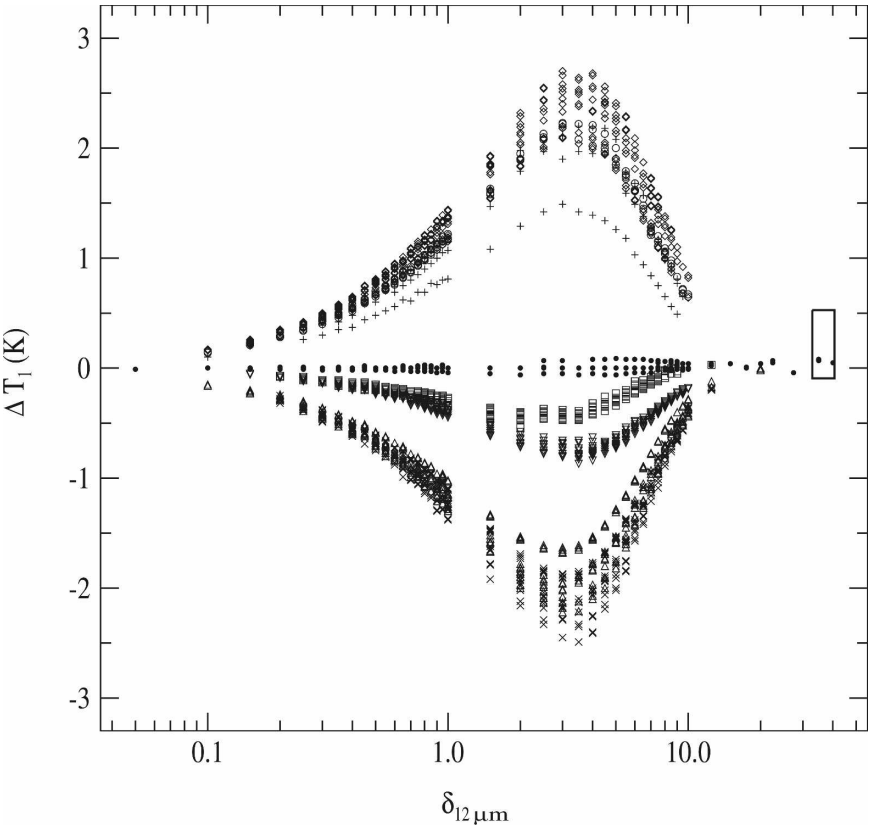

FIG. 9. Same as Fig. 8, but simulations are presented as a function of the optical thickness at 12 μm for an effective size of 40 μm.

individual ice crystals, used as an input for simulating T_1, T_2, and T_3. In the other cases, ΔT_1 gives an indication of the influence of the cloud model on brightness temperature at 8.7 μm; ΔT_1 has a magnitude ranging from 2 to 5 K, with a more important magnitude for particle effective sizes larger than 30 μm, showing the noticeable impact of the cloud model. It is important to notice that these variations are about ± 2 K and this influence should then be detected for spaceborne measurements. One can, however, notice that only four cloud models exhibit significantly differentiated BTD variations as a function of the effective size, suggesting that it is not necessary to use all the cloud models in cloud retrieval IIR algorithms. Similar behaviors of bullet rosettes and solid columns and those of hollow columns and spheroids can be explained from the single-scattering properties, which are quite similar for small particle size. Ambiguities occur between bullet rosettes and aggregates for a size of about 25 μm. This is different for effective diameters larger than 40 μm, where all shapes except aggregates and hollow columns can be differentiated. In addition, Fig. 8 confirms that temperature deviations due to the bimodal distribution are quite similar to those of individual ice crystals (see section 3c).

Certain categorization of particle shape should be achievable if the vertical profile of the shapes of particles does not substantially vary. Otherwise, the information about the vertical profile from polarized lidar measurements (Noël et al. 2002) may be useful for the analysis.

Figure 9 shows the temperature difference ΔT_1 between different particle shapes as a function of the optical thickness at 12 μm for an effective size of 40 μm. Assuming an accuracy threshold of ± 0.3 K, the influence of the particle shape could be observed from space measurements for semitransparent clouds with optical thicknesses ranging from 0.3 to 8 at 12 μm, with a maximum effect for optical thicknesses between 1 and 5. For a fixed particle shape, the impact of the size distribution is always smaller than 1 K and may be considered noise in IIR data analysis.

As far as IWP is concerned, the identification of the shape of cloud particles allows reducing the uncertainty in IWP retrieval. Using Eq. (5) and the appropriate values of coefficients a and b corresponding to the iden-

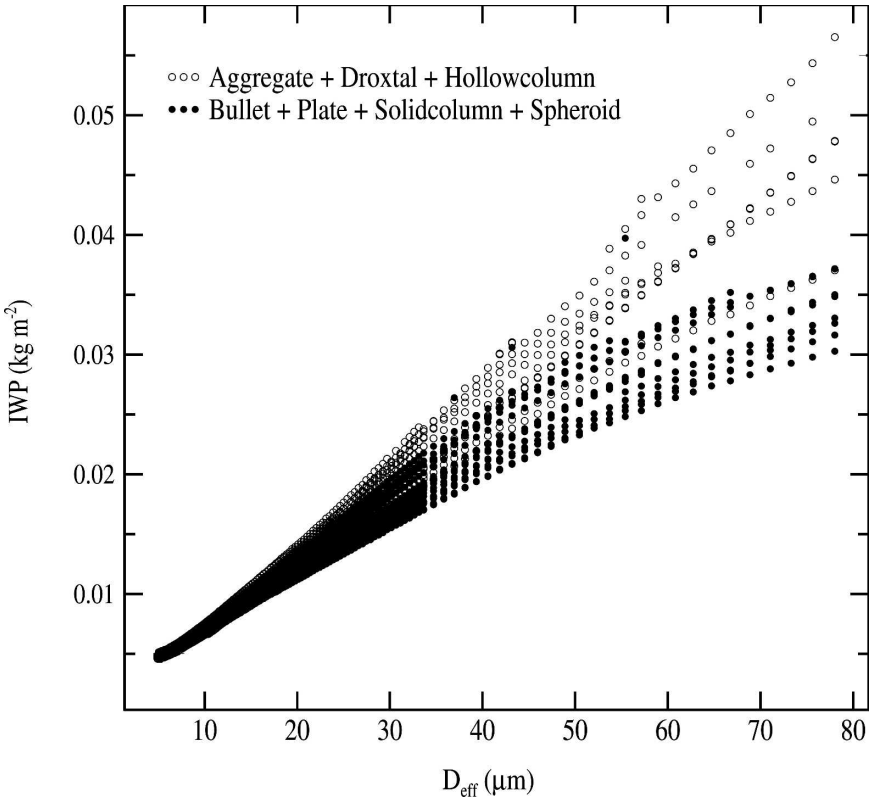

FIG. 10. IWP as a function of the effective size parameter D_{eff} for the seven particle shapes defined in Yang et al. (2005).

tified shapes, one can see from Fig. 10 that the error could be reduced to about ±15% for large IWP values.

A similar study has been performed on the basis of the simulations for the bottom of the atmosphere and 3-km altitude with the same conditions as in Fig. 8. The differences ΔT_1 are reported in Figs. 11, 12 as a function of the effective size and optical thickness, respectively. Figures 11 and 12 show very similar conclusions to those in the case for the top of the atmosphere. However, the magnitude of these differences is smaller in the cases shown in Figs. 11, 12. These results suggest that cloud characterization seems difficult with ground-based measurements. The choice of an observation station at higher altitudes or airborne measurements would minimize the atmospheric effect, especially the effect of water vapor.

Figure 13 shows the impact of the scattering on the brightness temperature at TOA at 8.7 and 10.6 μm. Deviations of the brightness temperatures have been calculated from the FASDOM code considering scattering or the absorption approximation (Fu et al. 1997). Figure 13a shows that scattering has important effects on the brightness temperature at 8.7 μm for optical thickness ranging between 1 and 10 and deviations can reach −10 K for small effective sizes. Figure 13a show that scattering has to be taken into account for a cloud model determination using the IIR channel 1 at 8.7 μm. At 10.6 μm, deviations are generally small and always less than 1 K for an effective size larger than 10 μm. In this case, scattering has a noticeable effect only for small particles with an optical thickness between 1 and 10. Note that the absorption approximation systematically overestimates the brightness temperature.

c. *Possible impact of atmospheric water vapor and ground temperature*

Table 2 presents the variation on the brightness temperature ΔT_1 simulated at the TOA in the 8.7-μm channel as a function of the water vapor content for various atmospheric models. In the case of moist atmospheres, Table 2 shows that accuracy better than ±10% in the water vapor content is needed for the characterization of semitransparent cloud ($\Delta T_1 < 0.5$ K). For the mid-latitude atmosphere, this constraint can be relaxed. But for dry atmospheres, such as in the polar regions, the accuracy on water vapor is not critical. Table 3 also confirms that atmospheric water vapor has an impor-

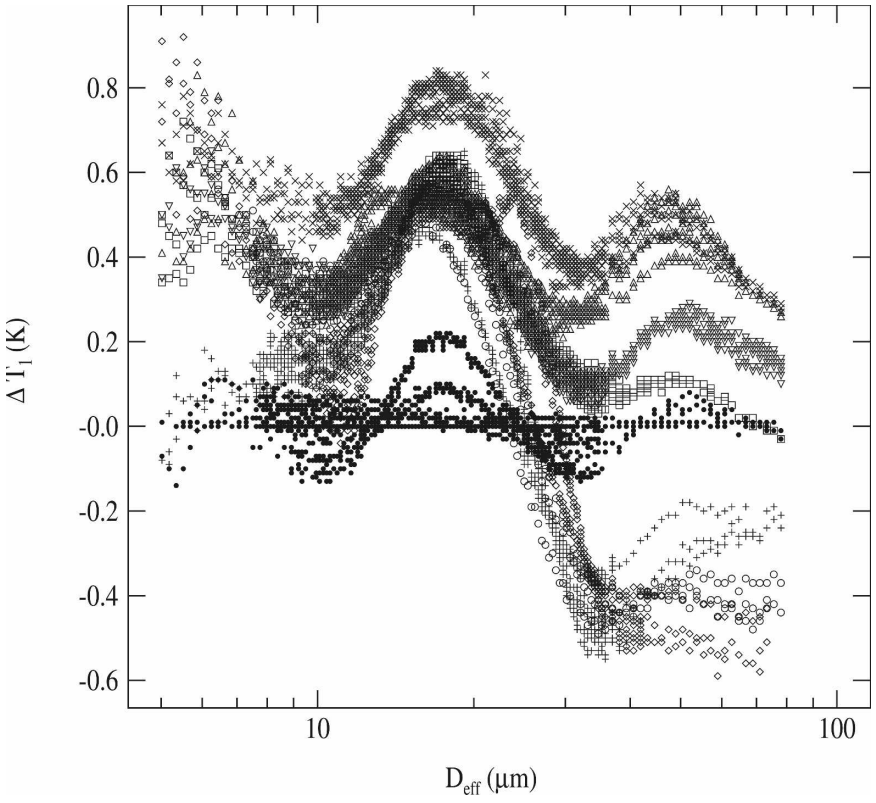

FIG. 11. Same as Fig. 8, but simulations are performed at the BOA.

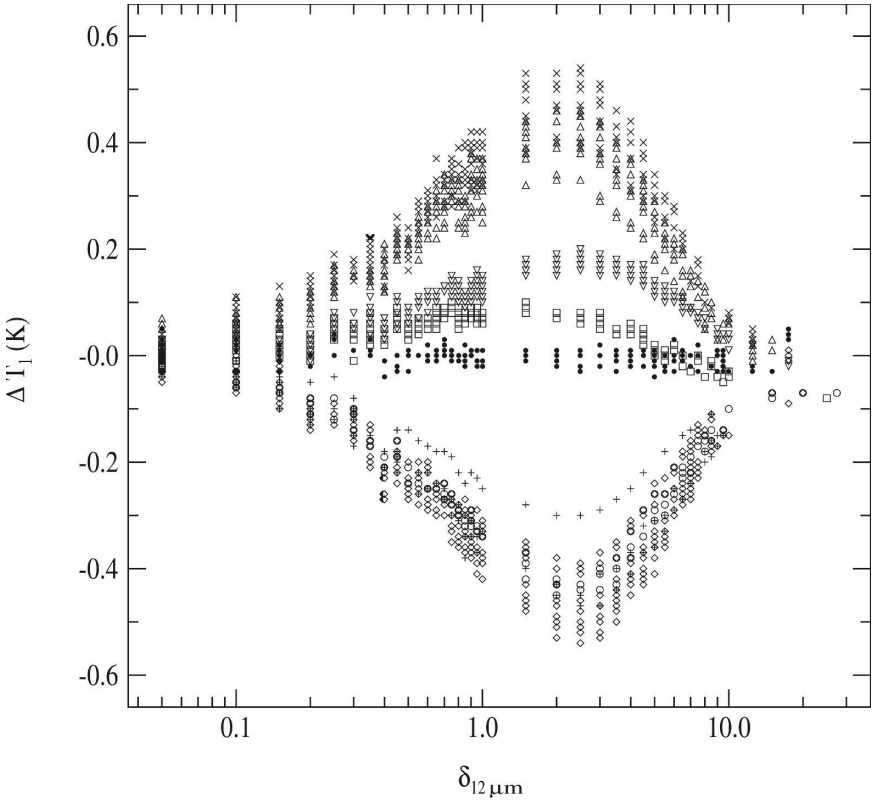

FIG. 12. Same as Fig. 9, but simulations are performed at the BOA.

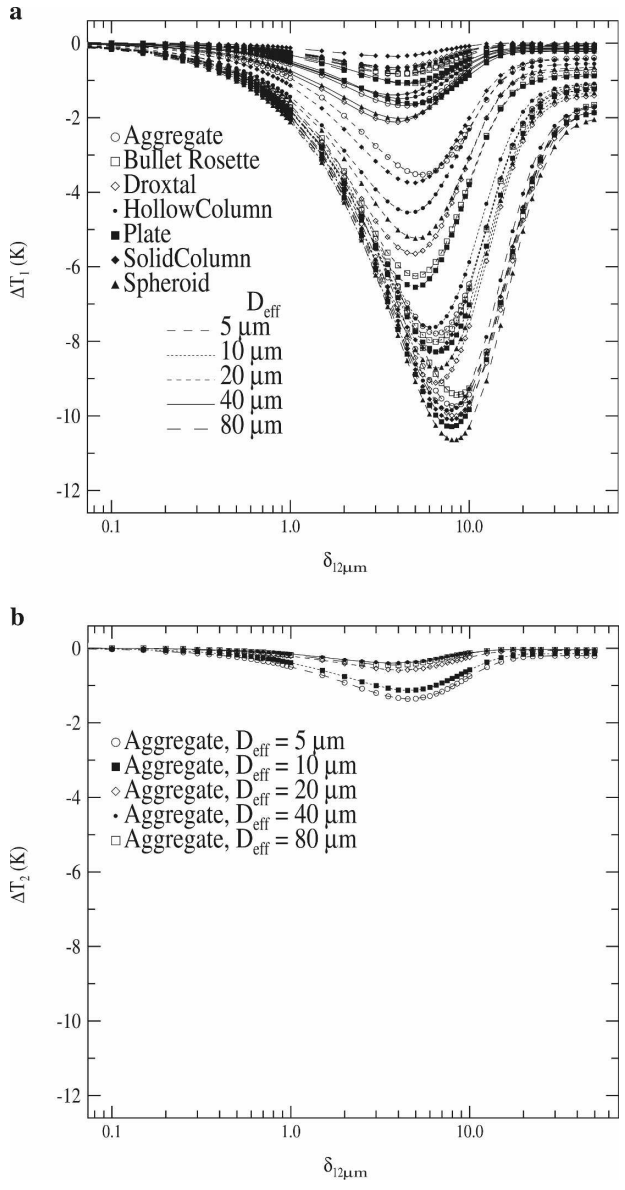

FIG. 13. Deviations $\Delta T = T_s - T_a$ on the brightness temperature at TOA due to scattering, as a function of cloud model. The T_s is calculated with FASDOM accounting for scattering; T_a is calculated without scattering, but considering that the cloud is not a purely absorbing media from the absorption approximation (Fu et al. 1997). (a) Deviations ΔT_1 in channel 1 (8.7 μm); (b) deviations ΔT_2 in channel 2 (10.6 μm). Note that the legends are different in (a) and (b).

tant influence on the brightness temperature simulated at the BOA. For moist atmospheres, Table 3 shows that an altitude of 5 km is required for accurate retrieval of cloud properties ($\Delta T_1 < 0.3$ K).

In the same manner, the variation of the brightness temperature ΔT_1 associated with the uncertainty of the cloud-top temperature ΔT_c, surface temperature ΔT_s, or surface emissivity $\Delta\varepsilon_s$ has been also estimated (Table 3). These results show that a precise knowledge of the atmospheric or surface parameter is necessary to obtain accurate retrievals. Without accurate data, the uncertainties on the brightness temperature in the 8.7-μm channel due to the atmospheric or surface parameters are on the order of those due to the cloud model. Consequently, the accurate retrieval of cloud microphysical parameters, and more particularly of particle shape, using the IIR channel at 8.7 μm is possible over the ocean and in areas for which additional data on surface or atmospheric profiles are available.

TABLE 2. Mean deviations on the brightness temperature ΔT_1 (K) simulated at the TOA in the 8.7-μm channel as a function of the cloud optical thickness δ_c, assuming a relative uncertainty ΔH_2O (10%, 25%, or 50%) on the water vapor content (reported in grams per centimeter squared), for various standard atmospheric models and cloud models defined in section 2.

		ΔT_1 (K)		
	ΔH_2O	$\delta_c = 0.25$	$\delta_c = 2$	$\delta_c = 5$
Tropical: 4.07 g cm^{-2}	10%	0.4	0.3	0.2
	25%	1.0	0.8	0.5
	50%	2.0	1.7	1.1
Midlatitude summer:	10%	0.2	0.2	0.1
2.91 g cm^{-2}	25%	0.6	0.5	0.3
	50%	1.2	1.0	0.7
Sub-Arctic summer:	10%	0.2	0.2	0.1
2.08 g cm^{-2}	25%	0.5	0.4	0.3
	50%	1.0	0.9	0.6
Midlatitude winter:	10%	0.1	<0.1	<0.1
0.85 g cm^{-2}	25%	0.2	0.1	0.1
	50%	0.3	0.3	0.2
Sub-Arctic winter:	10%	<0.1	<0.1	<0.1
0.42 g cm^{-2}	25%	<0.1	<0.1	<0.1
	50%	0.1	0.1	<0.1

TABLE 3. Mean deviations on the brightness temperature ΔT_1 (K) simulated under the same conditions as Table 2, but considering a tropical atmospheric profile and assuming an uncertainty of the cloud-top temperature ΔT_c, surface temperature ΔT_s, and surface emissivity $\Delta\varepsilon_s$. As a comparison, the influence of a relative uncertainty of 10% on the water vapor content ΔH_2O is also reported for calculations at the TOA, or under the cloud at the BOA or at higher altitudes (3 or 5 km).

	ΔT_1 (K)			
	$\delta_c = 0.5$	$\delta_c = 1$	$\delta_c = 5$	$\delta_c = 10$
$\Delta T_c = 1$ K	<0.1	0.1	0.5	0.8
$\Delta T_s = 1$ K	0.5	0.4	0.3	0.1
$\Delta\varepsilon_s = 0.01$	0.3	0.3	0.2	<0.1
ΔH_2O–TOA	0.3	0.3	0.2	0.1
ΔH_2O–BOA	3.0	2.7	2.3	1.8
ΔH_2O–3 km	0.9	0.7	0.5	0.3
ΔH_2O–5 km	0.3	0.2	0.1	0.1

5. Conclusions

The sensitivity of brightness temperature to the microphysical properties of ice cloud was studied. Brightness temperatures were calculated using a fast yet accurate radiative transfer code that accounts for gaseous absorption and multiple scattering. Spaceborne, airborne, and ground-based observations were simulated on the basis of the spectral responses similar to those for the three IIR channels. All parameters associated with cloud structure were assumed a priori. The main objective of the present study was to evaluate the impact of cloud microphysics (e.g., particle shape and size distribution). This effort was aimed at accessing the sensitivity of IIR measurements and evaluating the expected accuracy of the retrievals of the effective particle size, cloud optical depth, and ice water path.

From spaceborne observations, the two-channel (10.6 and 12 μm) split window technique allows the retrieval of cloud properties with an uncertainty of $\pm 10\%$ to $\pm 25\%$ for the effective size and about $\pm 10\%$ for the optical thickness. IWP depends on cloud model and the resulting uncertainty of IWP is on the order of $\pm 25\%$. This uncertainty is mainly due to the particle shape and, to a lesser extent, the size distribution. From a theoretical point of view, the use of the third channel (8.7 μm) allows for constraining the cloud model and improving the determination of effective particle size. Calculations showed that the sensitivity of the brightness temperature simulated at 8.7 μm is much larger than the expected IIR accuracy (approximately ± 0.3 K). Consequently, an indication of the cloud model could be reachable for semitransparent clouds with optical thicknesses ranging from 0.3 to 8. For extreme cloud optical thicknesses, the retrieval accuracy depends strongly on the knowledge and accuracy of atmospheric and surface parameters. However, simulations showed that it was difficult to differentiate the selected particle size distributions. Furthermore, the channel at 8.7 μm is able to constrain the cloud microphysical model and then to improve the retrievals of optical depth and effective particle radius for nonopaque clouds.

We also carried out sensitivity studies regarding the retrieval of cloud properties from ground-based infrared radiation. It was shown that the influence of the atmosphere is quite important. The sensitivity of brightness temperature to cloud properties is much weaker for moist atmospheres. Thus, accurate characterization of cloud optical and microphysical properties from ground-based observations requires accurate knowledge of the atmospheric water vapor content and accurate radiometric measurements. Observation stations at higher altitudes or airborne measurements would allow one to minimize the atmospheric effect.

Acknowledgments. The authors thank all members of the CALIPSO IIR working group for fruitful discussions and the Centre National d'Etudes Spatiales (CNES) for financial support. Ping Yang's research is supported by the U.S. National Science Foundation Physical Meteorology Program (ATM-0239605).

REFERENCES

Ackerman, S. W., W. Smith, J. Spinhirne, and H. Revercombe, 1990: The 27–28 October 1986 FIRE IFO cirrus case study: Spectral properties of cirrus clouds in the 8–12 μm window. *Mon. Wea. Rev.,* **118,** 2377–2388.

Arnott, W. P., Y. Dong, J. Hallett, and M. R. Poellot, 1994: Role of small ice crystals in radiative properties of cirrus: A case study, FIRE II, 22 November 1991. *J. Geophys. Res.,* **99,** 1371–1381.

Baran, A. J., 2003: Simulation of infrared scattering from ice aggregates by use of a size-shape distribution of circular ice cylinders. *Appl. Opt.,* **42,** 2811–2818.

——, J. S. Foot, and D. Mitchell, 1998: Ice-crystal absorption: A comparison between theory and implications for remote sensing. *Appl. Opt.,* **37,** 2207–2215.

Baum, B. A., D. P. Kratz, P. Yang, S. C. Ou, Y. Hu, P. Soulen, and S. C. Tsay, 2000: Remote sensing of cloud properties using MODIS Airborne Simulator imagery during SUCCESS: I. Data and models. *J. Geophys. Res.,* **105,** 11 767–11 780.

——, A. J. Heymsfield, P. Yang, and S. M. Bedka, 2005a: Bulk scattering properties for the remote sensing of ice clouds. Part I: Microphysical data and models. *J. Appl. Meteor.,* **44,** 1885–1895.

——, P. Yang, A. J. Heymsfield, S. Platnick, M. D. King, Y. X. Hu, and S. T. Bedka, 2005b: Bulk scattering properties for the remote sensing of ice clouds. Part II: Narrowband models. *J. Appl. Meteor.,* **44,** 1896–1911.

——, ——, S. L. Nasiri, A. K. Heidinger, A. J. Heymsfield, and J. Li, 2007: Bulk scattering properties for the remote sensing of ice clouds. Part III: High-resolution spectral models from 100 to 3250 cm^{-1}. *J. Appl. Meteor. Climatol.,* **46,** 423–434.

Chepfer, H., P. Goloub, J. Riedi, J. De Haan, J. W. Hovenier, and P. H. Flamant, 2001: Ice crystal shapes in cirrus clouds derived from POLDER-1/ADEOS. *J. Geophys. Res.,* **106,** 7955–7966.

Chiriaco, M., H. Chepfer, V. Noël, A. Delaval, M. Haeffelin, P. Dubuisson, and P. Yang, 2004: Improving retrievals of cirrus cloud particle size coupling lidar and three-channel radiometric techniques. *Mon. Wea. Rev.,* **132,** 1684–1700.

——, and Coauthors, 2007: Comparison of CALIPSO-like, LaRC, and MODIS retrievals of ice-cloud properties over SIRTA in France and Florida during CRYSTAL-FACE. *J. Appl. Meteor. Climatol.,* **46,** 249–272.

Chomette, O., A. Garnier, A. Lifermann, and J. Pelon, 2003: Retrieval of cloud emissivity and particle size in the frame of the CALIPSO mission. *Proc. IGARSS '03,* Toulouse, France, IEEE International, 1520–1522.

Chou, M., K. Lee, S. Q. Tsay, and Q. Fu, 1999: Parameterization for cloud longwave scattering for use in atmospheric models. *J. Climate,* **12,** 159–169.

Cooper, S. J., T. S. L'Ecuyer, and G. L. Stephens, 2003: The impact of explicit cloud boundary information on ice cloud microphysical property retrievals from infrared radiance. *J. Geophys. Res.,* **108,** 4107, doi:10.1029/2002JD002611.

Donovan, D. P., 2003: Ice-cloud effective size parameterization based on combined lidar, radar reflectivity, and mean Doppler velocity measurements. *J. Geophys. Res.,* **108,** 4573, doi:10.1029/2003JD003469.

Dubuisson, P., J.-C. Buriez, and Y. Fouquart, 1996: High spectral resolution solar radiative transfer in absorbing and scattering media: Application to the satellite simulation. *J. Quant. Spectrosc. Radiat. Transfer,* **55,** 103–126.

——, V. Giraud, O. Chomette, H. Chepfer, and J. Pelon, 2005: Fast radiative transfer modeling for infrared imaging radiometry. *J. Quant. Spectrosc. Radiat. Transfer,* **95,** 201–220.

Ebert, E. E., and J. A. Curry, 1992: A parameterization of cirrus cloud optical properties for climate models. *J. Geophys. Res.,* **97,** 3831–3836.

Foot, J. S., 1988: Some observations of the optical properties of clouds, II, Cirrus. *Quart. J. Roy. Meteor. Soc.,* **114,** 145–164.

Fu, Q., 1996: An accurate parameterization of the solar radiative properties of cirrus clouds for climate models. *J. Climate,* **9,** 2058–2082.

——, K. N. Liou, M. C. Cribb, T. P. Charlock, and A. Grossman, 1997: Multiple scattering parameterization in thermal infrared radiative transfer. *J. Atmos. Sci.,* **54,** 2799–2812.

——, P. Yang, and W. B. Sun, 1998: An accurate parameterization of the infrared radiative properties of cirrus clouds for climate models. *J. Climate,* **11,** 2223–2237.

——, W. B. Sun, and P. Yang, 1999: On modeling of scattering and absorption by nonspherical cirrus ice particles at thermal infrared wavelengths. *J. Atmos. Res.,* **56,** 2937–2947.

Gayet, J.-F., and Coauthors, 2006: Microphysical and optical properties of midlatitude cirrus clouds observed in the Southern Hemisphere during INCA. *Quart. J. Roy. Meteor. Soc.,* **132,** 2719–2748, doi:10.1256/qj.05.162.

Giraud, V., J.-C. Buriez, Y. Fouquart, F. Parol, and G. Sèze, 1997: Large-scale analysis of cirrus clouds from AVHRR data: Assessment of both a microphysical index and the cloud-top temperature. *J. Appl. Meteor.,* **36,** 664–675.

——, O. Thouron, J. Riedi, and P. Goloub, 2001: Cloud top temperature and infrared split window signature in relation with thermodynamic phase. *Geophys. Res. Lett.,* **28,** 983–986.

Heymsfield, A. J., A. Bansemer, P. R. Field, S. L. Durden, J. Stith, J. E. Dye, W. Hall, and T. Grainger, 2002: Observations and parameterizations of particle size distributions in deep tropical cirrus and stratiform precipitating clouds: Results from in situ observations in TRMM field campaigns. *J. Atmos. Sci.,* **59,** 3457–3491.

——, S. Matrosov, and B. Baum, 2003: Ice water path-optical depth relationships for cirrus and deep stratiform ice cloud layers. *J. Appl. Meteor.,* **42,** 1369–1390.

Inoue, T., 1985: On the temperature and effective emissivity determination of semi-transparent cirrus clouds by bi-spectral measurements in the window region. *J. Meteor. Soc. Japan,* **63,** 88–98.

——, 1987: A cloud type classification with NOAA 7 split-window measurements. *J. Geophys. Res.,* **92,** 3991–4000.

Ivanova, D., D. L. Mitchell, W. P. Arnott, and M. Poellot, 2001: A GCM parameterization for bimodal size spectra and ice mass removal rates in mid-latitude cirrus clouds. *Atmos. Res.,* **59,** 89–113.

King, M. D., S. Platnick, P. Yang, G. T. Arnold, M. A. Gray, J. C. Riédi, S. A. Ackerman, and K. N. Liou, 2004: Remote sensing of liquid water and ice cloud optical thickness, and effective radius in the Arctic: Application of airborne multispectral MAS data. *J. Atmos. Oceanic Technol.,* **21,** 857–875.

Kosarev, A. L., and I. P. Mazin, 1991: An empirical model of the physical structure of upper layer clouds. *Atmos. Res.,* **26,** 213–228.

Kratz, D. P., 1995: The correlated k-distribution technique as applied to the AVHRR channels. *J. Quant. Spectrosc. Radiat. Transfer,* **53,** 501–517.

Liou, K. N., 1986: Influence of cirrus clouds on weather and climate processes: A global perspective. *Mon. Wea. Rev.,* **114,** 1167–1199.

McClatchey, R. A., R. W. Fenn, J. E. A. Shelby, F. E. Voltz, and J. S. Garing, 1972: Optical properties of the atmosphere. Res. Paper AFCRF-72-0497, Hanscom Air Force Base, Bedford, MA, 108 pp.

McFarquhar, G. M., and A. J. Heymsfield, 1996: Microphysical characteristics of three anvils sampled during the Central Equatorial Pacific Experiment (CEPEX). *J. Atmos. Sci.,* **53,** 2401–2423.

Mitchell, D. L., 1991: Evolution of snow-size spectra in cyclonic storms. Part II: Deviations from the exponential form. *J. Atmos. Sci.,* **48,** 1885–1899.

——, 2002: Effective diameter in radiation transfer: General definition, applications, and limitations. *J. Atmos. Sci.,* **59,** 2330–2346.

——, and W. P. Arnott, 1994: A model predicting the evolution of ice particle size spectra and the radiative properties of cirrus clouds. Part II: Dependence of absorption and extinction on ice crystal morphology. *J. Atmos. Sci.,* **51,** 817–832.

——, A. Macke, and Y. Liu, 1996: Modeling cirrus clouds. Part II: Treatment of radiative properties. *J. Atmos. Sci.,* **53,** 2967–2988.

Noël, V., H. Chepfer, G. Ledanois, A. Delaval, and P. H. Flamant, 2002: Classification of particle shape ratios in cirrus clouds based on the lidar depolarization ratio. *Appl. Opt.,* **41,** 4245–4257.

Parol, F., J.-C. Buriez, G. Brogniez, and Y. Fouquart, 1991: Information content of AVHRR channel 4 and 5 with respect to the effective radius of cirrus cloud particles. *J. Appl. Meteor.,* **30,** 973–984.

Rädel, G., C. Stubenrauch, R. Holz, and D. L. Mitchell, 2003: Retrieval of effective ice crystal size in the infrared: Sensitivity study and global measurements from TIROS-N Operational Vertical Sounder. *J. Geophys. Res.,* **108,** 4281, doi:10.1029/2002JD002801.

Stamnes, K., S. C. Tsay, W. Wiscombe, and K. Jayaweera, 1988: Numerically stable algorithm for Discrete-Ordinate-Method radiative transfer in multiple scattering and emitting layered media. *Appl. Opt.,* **27,** 2502–2509.

Stephens, G. L., S. C. Tsay, P. W. Stackhose, and P. J. Flatau, 1990: The relevance of the microphysical and radiative properties of cirrus clouds to climate and climate feedback. *J. Atmos. Sci.,* **47,** 1742–1753.

Stubenrauch, C. J., R. Holz, A. Chédin, D. Mitchell, and A. J. Baran, 1999: Retrieval of cirrus ice crystal sizes from 8.3 and 11.1 μm emissivities determined by the improved initialization inversion of TIROS-N operational vertical sounder observations. *J. Geophys. Res.,* **104** (D24), 31 793–31 808.

Varley, D. J., 1978: Cirrus particle distribution study, part I. Air

Force Geophysical Laboratory Rep. AFGL-TR-78-0192, 71 pp.

Walko, R. L., W. R. Cotton, M. P. Meyers, and J. Y. Harrington, 1995: New RAMS cloud microphysics parameterization. Part I: The single-moment scheme. *Atmos. Res.,* **38,** 29–62.

Warren, S. G., 1984: Optical constants of ice from the ultraviolet to the microwave. *Appl. Opt.,* **23,** 1206–1225.

Winker, D. M., J. Pelon, and M. P. McCormick, 2003: The CALIPSO mission: Spaceborne lidar for observation of aerosols and clouds. *Lidar Remote Sensing for Industry and Environment Monitoring III,* U. N. Singh, T. Itabe, and Z. Liu, Eds., International Society for Optical Engineering (SPIE Proceedings, Vol. 4893), 1–11.

Yang, P., B. C. Gao, B. A. Baum, Y. Hu, W. Wiscombe, S. C. Tsay, D. M. Winker, and S. L. Nasiri, 2001: Radiative properties of cirrus clouds in the infrared (8-13 um) spectral region. *J. Quant. Spectros. Radiat. Transfer,* **70,** 473–504.

——, H. Wei, H. L. Huang, B. A. Baum, Y. X. Hu, G. W. Kattawar, M. I. Mishchenko, and Q. Fu, 2005: Scattering and absorption property database for nonspherical ice particles in the near- through far-infrared spectral region. *Appl. Opt.,* **44,** 5512–5523.